

Photonic topological Anderson insulators

Simon Stützer¹, Yonatan Plotnik², Yaakov Lumer³, Paraj Titum⁴, Netanel H. Lindner², Mordechai Segev², Mikael C. Rechtsman⁵ & Alexander Szameit^{1*}

The hallmark property of two-dimensional topological insulators is robustness of quantized electronic transport of charge and energy against disorder in the underlying lattice¹. That robustness arises from the fact that, in the topological bandgap, such transport can occur only along the edge states, which are immune to backscattering owing to topological protection. However, for sufficiently strong disorder, this bandgap closes and the system as a whole becomes topologically trivial: all states are localized and all transport vanishes in accordance with Anderson localization^{2,3}. The recent suggestion⁴ that the reverse transition can occur was therefore surprising. In so-called topological Anderson insulators, it has been predicted⁴ that the emergence of protected edge states and quantized transport can be induced, rather than inhibited, by the addition of sufficient disorder to a topologically trivial insulator. Here we report the experimental demonstration of a photonic topological Anderson insulator. Our experiments are carried out in an array of helical evanescently coupled waveguides in a honeycomb geometry with detuned sublattices. Adding on-site disorder in the form of random variations in the refractive index of the waveguides drives the system from a trivial phase into a topological one. This manifestation of topological Anderson insulator physics shows experimentally that disorder can enhance transport rather than arrest it.

In parallel to investigations into electronic topological insulators, the recent demonstration of photonic topological insulators^{5–7} has shown that topological phenomena are not limited to the motion of electrons in solid-state materials. In fact, topological protection is a general wave phenomenon that applies equally well to many wave systems, including electromagnetic waves^{5–15}, acoustic waves^{16,17}, mechanical waves^{18,19} and cold atoms^{20,21}. Among these, photonic topological systems have been found to be useful in demonstrating effects that would otherwise be unreachable in the context of condensed-matter physics, such as Anderson localization^{22,23}, very strong strain²⁴, non-Hermitian behaviour²⁵ and the concept of topological bound states in the continuum²⁶. Furthermore, topological photonic systems provide a complementary set of potential technological applications, including new mechanisms for integrated optical isolation and general robustness to imperfections in the fabrication of photonic devices.

Here we demonstrate a topological Anderson insulator. Our experiments are carried out in a photonic platform, as proposed theoretically²⁷, based on a two-dimensional time-reversal-symmetry-broken Floquet topological insulator. In particular, when sufficient disorder is introduced, we enter the topological phase and observe unidirectional edge transport. Our key result, which demonstrates the possibility of inducing a topological phase using disorder, is universal and carries over to different dimensions²⁸ and to symmetry-protected topological phases^{4,35}. The experimental platform that we use is an array of evanescently coupled helical waveguides²⁹, where the diffraction of light through the system is described by the paraxial wave equation, which is mathematically equivalent to the Schrödinger equation. A closely related system has been used for the observation of Floquet photonic topological insulators⁵.

To explain the mechanism that underlies our photonic topological Anderson insulator, we start with a honeycomb lattice of helical waveguides⁵, which is a photonic Floquet topological insulator. The equation that describes the diffraction of a paraxial beam of light in this lattice can be written, under the tight-binding approximation, as

$$i\partial_z\psi_i = c \sum_{j(\text{nni})} e^{-iA(z)\cdot r_{ij}}\psi_j + m_\delta\delta_i\psi_i \equiv \sum_j \hat{H}_{ij}(z)\psi_j \quad (1)$$

where z is the distance of propagation along the waveguide axis, ψ_i is the envelope function of the electric field in the i th waveguide, c is the coupling strength between waveguides, $A(z) = kR\Omega a(\cos(\Omega z), \sin(\Omega z), 0)$ is the gauge field induced by the helicity, k is the wavenumber of the light in the medium (fused silica), R is the radius of the helix, Ω is the longitudinal frequency associated with the helix, a is the nearest-neighbour spacing and r_{ij} is the displacement vector pointing from waveguide i to waveguide j . The honeycomb lattice comprises two triangular sublattices. The parameter δ_i takes the value 1 in one sublattice and -1 in the other, such that the on-site energies of the two are separated by the detuning $2m_\delta$. Equation (1) defines $\hat{H}(z)$ as the Hamiltonian at propagation distance z , and the summation therein is taken over nearest-neighbour waveguides. This is exactly the Schrödinger equation, where z takes the role of time. Because $A(z)$ is z -dependent and periodic, solutions to equation (1) can be obtained by using Floquet's theorem. Thus, the band structure can be obtained by diagonalizing the unitary evolution operator for one period³⁰. Detuning the two triangular sublattices breaks the inversion symmetry of the structure and opens a trivial bandgap. This can be quantified with a mass m_δ associated with the effective Dirac equation of the honeycomb lattice in the absence of the periodic driving. In the undetuned case ($m_\delta = 0$), the Dirac-cone dispersion is equivalent to that of massless relativistic particles. Such detuning can be realized experimentally in waveguide arrays by allowing the two honeycomb sublattices to have different refractive indices.

The mechanism according to which we realize the photonic topological Anderson insulator is depicted schematically in Fig. 1a. The band structure of the honeycomb lattice with straight and identical waveguides, so that the induced gauge field $A(z) = \mathbf{0}$ and $m_\delta = 0$, is shown in Fig. 1b. This band structure corresponds to that of a ribbon (associated with the zigzag edge of graphene³¹). As known in graphene physics, the ribbon band structure exhibits two Dirac cones (red ellipses in Fig. 1b) that are connected by a flat band of edge states³¹. When the waveguides follow a helical trajectory such that $A(z)$ is non-zero (Fig. 1c), the z -reversal symmetry is broken and a bandgap opens. In this case, each valley acquires an opposite mass: m_r and $-m_r$ for the left and right valleys, respectively. These opposite masses imply that the edge states cross the bandgap, with each edge state localized to opposite sides of the ribbon. Therefore, the bandgap is topological; the edge states form a single backscattering-free chiral edge state that is localized to the edge of the structure. This is the essence of a Floquet topological insulator in the honeycomb system⁵.

¹Institute for Physics, Rostock University, Rostock, Germany. ²Physics Department and Solid State Institute, Technion – Israel Institute of Technology, Haifa, Israel. ³Department of Electrical and Systems Engineering, University of Pennsylvania, Philadelphia, PA, USA. ⁴Joint Quantum Institute and Joint Center for Quantum Information and Computer Science, NIST/University of Maryland, College Park, MD, USA. ⁵Department of Physics, The Pennsylvania State University, University Park, PA, USA. *e-mail: alexander.szameit@uni-rostock.de

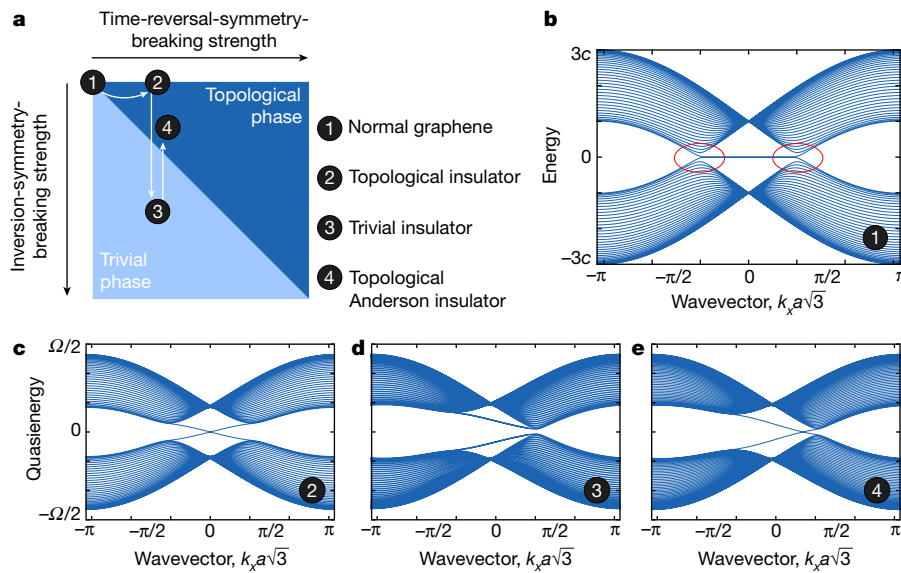


Fig. 1 | Floquet topological Anderson insulator in a detuned honeycomb lattice.

a, Mechanism for realizing the topological insulator phase in a photonic waveguide lattice. The white arrows indicate the trajectory through the phase diagram in the experimental protocol. The parameters for the band-structure calculations are chosen for illustration purposes. **b**, Band structure for a trivial honeycomb lattice with straight waveguides. The red ellipses indicate the Dirac cones. **c**, Time-reversal

Consider now what happens when the sublattices of the Floquet topological insulator are detuned so that the two sublattices exhibit different refractive indices. Introducing non-zero detuning breaks the inversion symmetry of the lattice, which adds a positive mass term m_δ to each valley. If the detuning is large enough ($m_\delta > m_\tau$), then the masses $m_\tau + m_\delta$ and $-m_\tau + m_\delta$ in both valleys become positive and the bandgap becomes trivial (Fig. 1d). In other words, the outcome of a sufficiently detuned honeycomb lattice of helical waveguides is a topologically trivial system with broken inversion and time-reversal symmetry. This is where disorder comes into play: as was recently proposed²⁷, this system can be brought into a topologically non-trivial phase using disorder. More specifically, it has been shown²⁷ (using the Born approximation) that introducing on-site disorder, which is achieved by randomizing the refractive-index contrasts of the waveguides, causes an effective decrease in the detuning m_δ . The decrease in m_δ grows stronger as the strength of the disorder is increased. Therefore, upon introducing disorder and increasing its strength, the mobility gap closes when $m_\tau = m_\delta$ and reopens for $m_\tau > m_\delta$. When the gap reopens, the system is topological (Fig. 1e). This is precisely the effect of photonic topological Anderson insulators: adding disorder brings the system from being topologically trivial ($m_\delta > m_\tau$) to topologically non-trivial ($m_\tau > m_\delta$).

A schematic depiction of the waveguide configuration is shown in Fig. 2a. In this setting, it is essential to control which states are excited. We do that by adding a one-dimensional auxiliary array—a ‘straw’—through which we selectively excite the modes of the system at a fixed energy (k_z). More specifically, in a one-dimensional waveguide array, tilting the phase front of the wave that illuminates the input facet determines the momentum of the excited Bloch mode. Here, such selective excitation is especially important because we would like to excite states entirely within the gap, to determine whether the gap exists and whether it is trivial or topological. By controlling the tilt angle of input of the beam, we can control k_x , the Bloch wavevector in the horizontal direction. The band structure (k_z versus k_x) of the straw is shown in the inset in Fig. 2a. We fix k_z (the Floquet quasienergy) by choosing k_x , and k_z is conserved as the beam travels through the straw and enters the honeycomb array. Thus, simply by changing the incidence angle of the beam, we can tune the quasienergy of the modes that are excited in the structure.

symmetry is broken by helical waveguide trajectories, opening a topological bandgap. **d**, Breaking the parity symmetry of the structure by detuning the sublattices sufficiently causes a trivial bandgap to form. **e**, Sufficiently strong disorder suppresses the effect of the parity-symmetry-breaking terms and moves the system into the topological Anderson insulator phase. The band structure shown in this case is for illustration purposes; there is no well defined band structure in the disordered case.

The bandwidth in k_z of the straw depends on k_x and is relatively wide (determined by the number of sites in the straw and input beam), limiting our ability to perform precise spectroscopy. However, it remains a highly useful tool for selective excitation of wave packets in the honeycomb lattice.

We first consider a system that breaks z -reversal symmetry ($m_\tau \neq 0$) with identical (non-detuned) waveguides ($m_\delta = 0$), and repeat the previous realization of a Floquet topological insulator⁵ (see Methods for details). Owing to the helicity of the waveguides, the system has a topological bandgap at quasienergy $k_z = 0$, and we expect to find a chiral edge state in this bandgap (the Floquet band structure is shown in the inset to Fig. 2a). This is precisely what we see. In Fig. 2b we show the output facet of the array in the case where k_z lies in the bandgap (top) and the case where it lies in the band (bottom). When k_z is in the gap, a chiral edge state is excited: the optical wave packet is launched from the straw and couples to the chiral edge state, where it propagates unidirectionally upwards in a clockwise direction around the honeycomb lattice, but does not penetrate into the lattice. On the other hand, when k_z lies in the band, the wave packet couples to bulk states; hence, it penetrates into the lattice and spreads into the array, so does not stay confined to the edge. The evolution of the edge state is shown in Fig. 2c. As the input beam is brought closer to the array, the edge state travels farther along the edge until it passes the top corner. The fact that it moves only upwards, and stays confined to the edge, is a signature of the chirality of the edge state. We note that for the choice of parameters of the waveguide array used in the experiment the longitudinal frequency of the helix Ω is smaller than the total bandwidth (6c) in the absence of the helix. This results in an additional topological gap, which opens at a quasienergy of around $k_z = \Omega/2$ and hosts chiral edge states, as shown in Fig. 2a. However, by using the selective excitation through the straw, in this experiment we always excite states with quasienergies close to $k_z = 0$ and do not probe states with quasienergy near $k_z = \Omega/2$.

We now describe the probing of a series of helical photonic lattices, where we introduce detuning between the sublattices ($m_\delta \neq 0$) of the honeycomb structure by making their refractive indices different. In practice, this is done by changing the speed of the laser-writing beam during the fabrication process (a higher writing speed results in a lower refractive index of the waveguides). In a series of six waveguide arrays, we systematically increase this detuning, decreasing the gap size as

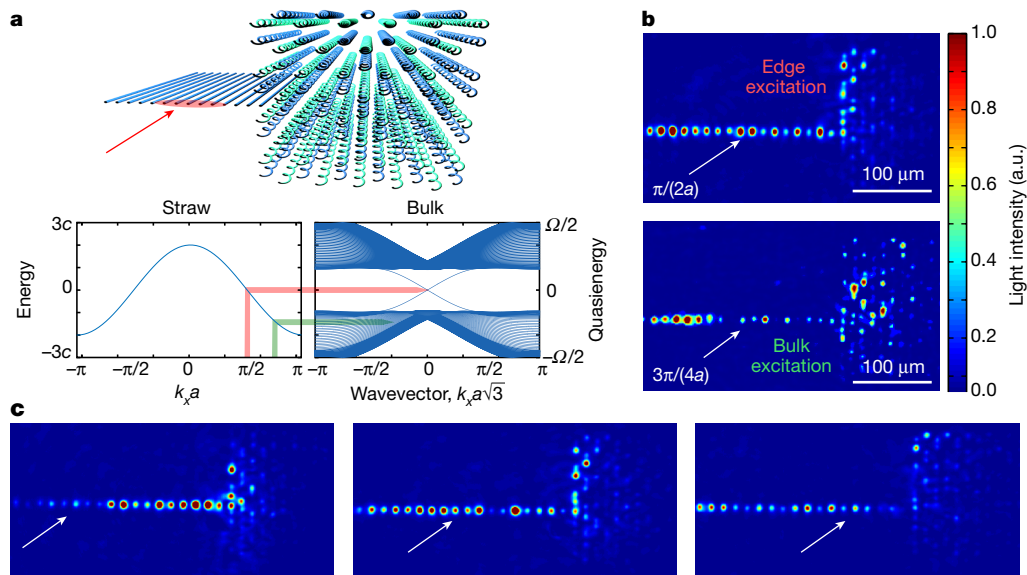


Fig. 2 | Set-up and functionality of the lattice system. **a**, Hybrid structure composed of a one-dimensional straw and a two-dimensional honeycomb lattice of helical waveguides (top), along with the corresponding dispersion relations (bottom). **b**, Determining the correct input angle for the incident light, such that a chiral edge state in the topological gap is excited. Two experimental images are shown, for $k_x = \pi/(2a)$ and $k_x = 3\pi/(4a)$;

m_δ increases, and examine how much the wavefunction launched through the straw penetrates into the lattice (plotted in Fig. 3). To do that, we choose $k_x = \pi/(2a)$, where the Bloch wavenumber in the

the excitation in the dispersion relation is sketched in the bottom plots of **a**. If the launch angle does not correspond to excitation in the gap, extensive coupling into the lattice bulk is observed. a.u., arbitrary units. **c**, Changing the input position (indicated by the white arrows) facilitates the observation of the evolution of the edge states as they propagate along the edge and pass the upper corner, never penetrating into the bulk.

straw corresponds to the value of k_z in the centre of the bandgap of the honeycomb lattice. For sufficiently strong detuning m_δ , we observe a sharp decrease in the penetration of light along the edge, which corresponds to the closing of the topological bandgap and the reopening of the trivial bandgap at $k_z = 0$. This observation constrains m_δ to be larger than 1.57 cm^{-1} , although precise determination of the on-site waveguide propagation constants within the array is not possible (owing to the exponential sensitivity of the refractive index to write speed and the effect of the lattice environment on the individual waveguides). Indeed, in the trivial gap, no states are present, and there is a dramatic drop in the penetration into the array along the edge. The inability to couple to edge states establishes that we have introduced sufficiently strong detuning, m_δ , to have opened the trivial bandgap, which does not support edge modes.

Next, we introduce on-site disorder and demonstrate the formation of the photonic topological Anderson insulator by observing whether the mid-gap excitation gives rise to coupling to a topological edge state. The disorder enters equation (1) on the right-hand side via an additional term, $wr_i\psi_i$, where r_i is a uniformly distributed random variable between -0.5 and 0.5 and w is the strength of the disorder. We find that for sufficiently strong disorder (corresponding to a maximum variation in laser write speed of 8 mm min^{-1}), the mid-gap excitation is able to couple into the lattice, staying largely confined to the edge (see Fig. 4a–c). As we move the input beam closer to the array, the light coupled into the array propagates farther along the edge, much as in the non-disordered topological system (with $m_\delta = 0$) of Fig. 2c. The beam moves up along the left edge, implying the presence of a chiral edge state (that was not present when the system was not disordered). We find the group velocity of the edge state to be $21 \mu\text{m cm}^{-1}$. We fit the profile of the excited wavefunction and find that it decays exponentially away from the edge, consistent with having excited predominantly the edge states (see Methods). For comparison, we show the same scenario but with no disorder and with the same m_δ in Fig. 4d–f. When no disorder is present, there is no observable edge excitation and minimal bulk penetration; that is, the beam launched into the topologically trivial photonic bandgap is reflected. The small amount of bulk penetration seen in Fig. 4d–f probably arises from the finite bandwidth of the input beam in k_z . The appearance of the chiral edge state when the disorder is sufficiently strong is evidence of the photonic

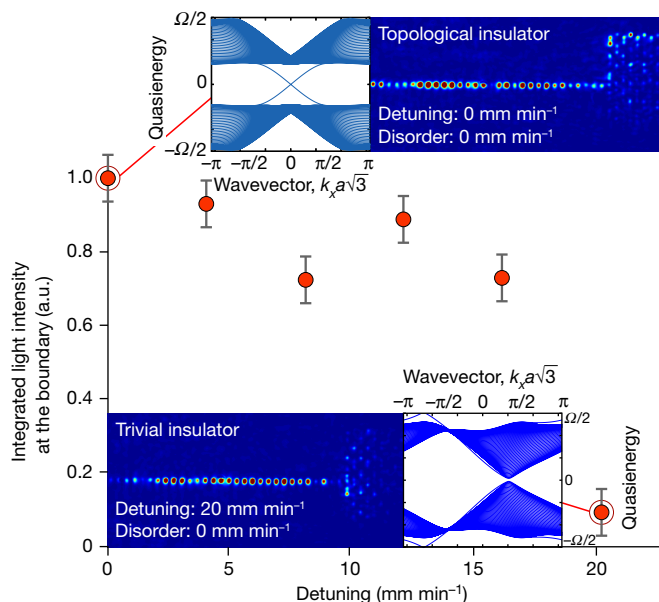


Fig. 3 | Engineering the topologically trivial phase. For sufficiently strong detuning between the sublattices of the honeycomb lattice, a trivial gap opens, such that the chiral edge state ceases to exist and all incident light is reflected back into the straw. The experiments show the light-intensity pattern as it exits the helical waveguide array (insets; colour scale as in Fig. 2) and the measured integrated intensity at the boundary as a function of detuning (main panel; in units of translation velocity of the writing laser). For zero detuning, the incident light resides only on the edge (indicating the topological insulator phase). When the detuning is small, the system is still in the topological phase and almost all the incident light resides on the edge. When the detuning is increased further, the system becomes topologically trivial and the incident light does not penetrate along the edge. There is no disorder in this lattice. The error bars indicate measurement uncertainty, and the confidence interval is about 0.06 of the maximum intensity observed (normalized to unity).

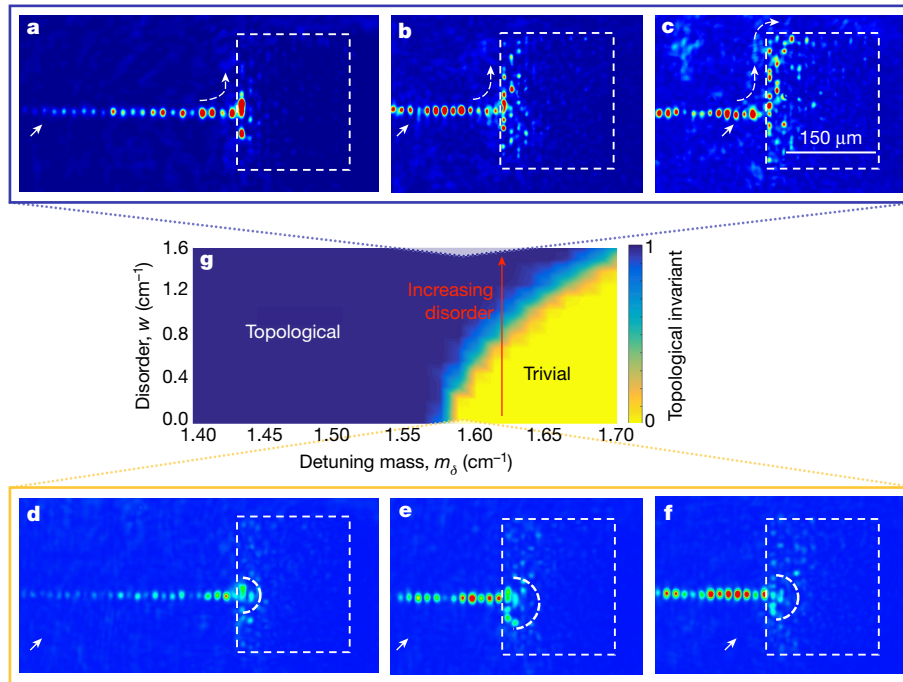


Fig. 4 | Formation of the photonic topological Anderson insulator. **a–c**, When sufficient disorder is added, the system is driven into the topological Anderson insulator phase and chiral edge states form. This is demonstrated by moving the excitation in the straw (solid arrows) close to the (disordered) honeycomb lattice, so that the edge state crawls up the edge (dashed arrows). The excitation in the straw is far from the honeycomb lattice (22 waveguides away; **a**); the excitation is at an intermediate distance from the lattice (11 waveguides away; **b**); and the excitation is close to the lattice (4 waveguides away; **c**). The dashed boxes indicate the honeycomb waveguide array. **d–f**, By contrast, in the fully ordered, detuned helical honeycomb lattice, essentially all light is

reflected into the straw, with only a small part penetrating into the bulk without exciting any edge mode. The excitation in the straw is far from the honeycomb lattice (**d**); the excitation is at an intermediate distance from the lattice (**e**); and the excitation is close to the lattice (**f**) (distances as in **a–c**). **g**, Phase diagram showing the trivial and topological phases as a function of the detuning mass, m_δ , and disorder strength, w , obtained using experimental parameters (see Methods). The red arrow indicates the trajectory through the phase diagram as the system starts from the trivial phase and enters the topological phase with increasing disorder strength.

topological Anderson insulator phase²⁷. In Fig. 4g we show a phase diagram that indicates the topological invariant that counts the number of edge states at quasienergy $k_z = 0$ as a function of detuning m_δ and disorder strength w (a full description of the topological invariant^{32,33} that we use is provided in Methods). The phase diagram shows that adding sufficiently strong disorder to the detuned lattice in the trivial phase necessarily takes the system into the topological phase. For considerably stronger disorder, localization sets in, making the system Anderson-localized⁴.

The experiments presented here demonstrate the observation of a topological Anderson insulator using a photonic platform. Specifically, we have shown that a topologically trivial system can undergo a transition and become topological when disorder is added. This was carried out by observing the emergence of a chiral edge state upon introducing sufficiently strong disorder (where there was none with no disorder). The topological Anderson insulator phase is a clear example of the complex relationship between topology and disorder: it goes beyond the usual notion whereby sufficiently strong disorder destroys topologically protected transport¹. It shows that disorder is a key variable in probing topological phases, in the sense that even in trivial systems topological behaviour can emerge when disorder is introduced at sufficient strengths. We expect that our experimental realization of this phase will stimulate a range of theoretical and experimental studies to explore the role of disorder in topological systems. This prompts various important questions, such as what happens to the topological Anderson insulator phase in the presence of interactions in optical, atomic and condensed-matter systems, and whether there is a topological Anderson insulator phase in the quantum many-body regime. The answers to these questions are now being brought within experimental reach.

After this paper was submitted, a related paper³⁴ appeared on arXiv that reported the observation of a topological Anderson insulator in one-dimensional atomic wires.

Online content

Any Methods, including any statements of data availability and Nature Research reporting summaries, along with any additional references and Source Data files, are available in the online version of the paper at <https://doi.org/10.1038/s41586-018-0418-2>.

Received: 18 October 2017; Accepted: 20 June 2018;
Published online 22 August 2018.

- Hasan, M. Z. & Kane, C. L. Colloquium: Topological insulators. *Rev. Mod. Phys.* **82**, 3045–3067 (2010).
- Anderson, P. W. Absence of diffusion in certain random lattices. *Phys. Rev.* **109**, 1492–1505 (1958).
- Segev, M., Silberberg, Y. & Christodoulides, D. N. Anderson localization of light. *Nat. Photon.* **7**, 197–204 (2013).
- Li, J., Chu, R.-L., Jain, J. K. & Shen, S.-Q. Topological Anderson insulator. *Phys. Rev. Lett.* **102**, 136806 (2009).
- Rechtsman, M. C. et al. Photonic Floquet topological insulators. *Nature* **496**, 196–200 (2013).
- Hafezi, M., Mittal, S., Fan, J., Migdall, A. & Taylor, J. M. Imaging topological edge states in silicon photonics. *Nat. Photon.* **7**, 1001–1005 (2013).
- Cheng, X. et al. Robust reconfigurable electromagnetic pathways within a photonic topological insulator. *Nat. Mater.* **15**, 542–548 (2016).
- Haldane, F. D. M. & Raghu, S. Possible realization of directional optical waveguides in photonic crystals with broken time-reversal symmetry. *Phys. Rev. Lett.* **100**, 013904 (2008).
- Wang, Z., Chong, Y., Joannopoulos, J. D. & Soljacic, M. Observation of unidirectional backscattering-immune topological electromagnetic states. *Nature* **461**, 772–775 (2009).
- Umucalilar, R. O. & Carusotto, I. Artificial gauge field for photons in coupled cavity arrays. *Phys. Rev. A* **84**, 043804 (2011).

11. Hafezi, M., Demler, E. A., Lukin, M. D. & Taylor, J. M. Robust optical delay lines with topological protection. *Nat. Phys.* **7**, 907–912 (2011).
12. Fang, K., Yu, Z. & Fan, S. Realizing effective magnetic field for photons by controlling the phase of dynamic modulation. *Nat. Photon.* **6**, 782–787 (2012).
13. Khanikaev, A. B. et al. Photonic topological insulators. *Nat. Mater.* **12**, 233–239 (2013).
14. Maczewsky, L. J., Zeuner, J. M., Nolte, S. & Szameit, A. Observation of photonic anomalous Floquet topological insulators. *Nat. Commun.* **8**, 13756 (2017).
15. Mukherjee, S. et al. Experimental observation of anomalous topological edge modes in a slowly driven photonic lattice. *Nat. Commun.* **8**, 13918 (2017).
16. Khanikaev, A. B., Fleury, R., Mousavi, S. H. & Alù, A. Topologically robust sound propagation in an angular-momentum-biased graphene-like resonator lattice. *Nat. Commun.* **6**, 8260 (2015).
17. Yang, Z. et al. Topological acoustics. *Phys. Rev. Lett.* **114**, 114301 (2015).
18. Süssstrunk, R. & Huber, S. D. Observation of phononic helical edge states in a mechanical topological insulator. *Science* **349**, 47–50 (2015).
19. Nash, L. M. et al. Topological mechanics of gyroscopic metamaterials. *Proc. Natl Acad. Sci. USA* **112**, 14495–14500 (2015).
20. Jotzu, G. et al. Experimental realization of the topological Haldane model with ultracold fermions. *Nature* **515**, 237–240 (2014).
21. Aidelsburger, M. et al. Measuring the Chern number of Hofstadter bands with ultracold bosonic atoms. *Nat. Phys.* **11**, 162–166 (2014).
22. Schwartz, T., Bartal, G., Fishman, S. & Segev, M. Transport and Anderson localization in disordered two-dimensional photonic lattices. *Nature* **446**, 52–55 (2007).
23. Lahini, Y. et al. Anderson localization and nonlinearity in one-dimensional disordered photonic lattices. *Phys. Rev. Lett.* **100**, 013906 (2008).
24. Rechtsman, M. C. et al. Strain-induced pseudomagnetic field and photonic Landau levels in dielectric structures. *Nat. Photon.* **7**, 153–158 (2013).
25. Weimann, S. et al. Topologically protected bound states in photonic parity-time-symmetric crystals. *Nat. Mater.* **16**, 433–438 (2017).
26. Plotnik, Y. et al. Experimental observation of optical bound states in the continuum. *Phys. Rev. Lett.* **107**, 183901 (2011).
27. Titum, P., Lindner, N. H., Rechtsman, M. C. & Refael, G. Disorder-induced Floquet topological insulators. *Phys. Rev. Lett.* **114**, 056801 (2015).
28. Guo, H.-M., Rosenberg, G., Refael, G. & Franz, M. Topological Anderson insulator in three dimensions. *Phys. Rev. Lett.* **105**, 216601 (2010).
29. Szameit, A. & Nolte, S. Discrete optics in femtosecond-laser-written photonic structures. *J. Phys. B* **43**, 163001 (2010).
30. Lindner, N. H., Refael, G. & Galitski, V. Floquet topological insulator in semiconductor quantum wells. *Nat. Phys.* **7**, 490–495 (2011).
31. Castro Neto, A. H., Guinea, F., Peres, N. M. R., Novoselov, K. S. & Geim, A. K. The electronic properties of graphene. *Rev. Mod. Phys.* **81**, 109–162 (2009).
32. Rudner, M. S., Lindner, N. H., Berg, E. & Levin, M. Anomalous edge states and the bulk-edge correspondence for periodically driven two-dimensional systems. *Phys. Rev. X* **3**, 031005 (2013).
33. Titum, P., Berg, E., Rudner, M. S., Refael, G. & Lindner, N. H. Anomalous Floquet-Anderson insulator as a nonadiabatic quantized charge pump. *Phys. Rev. X* **6**, 021013 (2016).
34. Meier, E. J. et al. Observation of the topological Anderson insulator in disordered atomic wires. Preprint at <https://arxiv.org/abs/1802.02109> (2018).
35. Groth, C. W. et al. Theory of the topological Anderson insulator. *Phys. Rev. Lett.* **103**, 196805 (2019).

Acknowledgements A.S. and M.S. thank the German-Israeli DIP (project BL 574/13-1). A.S. acknowledges funding from the German Research Foundation (project SZ 276/9-1). M.S. thanks the European Research Council for financial support. N.L. acknowledges financial support from the European Research Council under the European Union Horizon 2020 Research and Innovation Programme (grant agreement number 639172), from the People Programme (Marie Curie Actions) of the European Union's Seventh Framework Programme (FP7/2007-2013) under REA grant agreement number 631696 and from the Israeli Center of Research Excellence (I-CORE) Circle of Light, funded by the Israeli Science Foundation. M.C.R. acknowledges support from the National Science Foundation under grant number DMS-1620422, as well as the Sloan (FG-2016-6418) and Kaufman (KA2017-91788) foundations. P.T. is supported by an NRC postdoctoral fellowship. The authors acknowledge the University of Maryland supercomputing resources made available for conducting the research reported in this paper.

Author contributions All authors contributed substantially to this work.

Competing interests The authors declare no competing interests.

Additional information

Extended data is available for this paper at <https://doi.org/10.1038/s41586-018-0418-2>.

Reprints and permissions information is available at <http://www.nature.com/reprints>.

Correspondence and requests for materials should be addressed to A.S.

Publisher's note: Springer Nature remains neutral with regard to jurisdictional claims in published maps and institutional affiliations.

METHODS

Details of the fabricated lattice. In our waveguide structures, we use a helix pitch of $Z = 1$ cm, a radius of $R = 10$ μm and a nearest-neighbour spacing of $a = 14$ μm ; at our probe wavelength ($\lambda = 633$ nm), this corresponds to a dimensionless gauge field strength of $|A| = kR\Omega a = 1.26$, with $k = 2\pi n_0/\lambda$, $\Omega = 2\pi/Z$, an ambient refractive index $n_0 = 1.45$ and $a = 14$ μm nearest-neighbour spacing, which gives rise to a nearest-neighbour coupling strength of 1.8 cm^{-1} . The waveguides are written at an average writing speed of 90 mm min^{-1} . A broad input probe beam is incident on the straw, with a beam waist of approximately 100 μm .

Discussion of the topological invariant that characterizes the photonic topological Anderson insulator phase. The topological invariant that characterizes the non-interacting two-dimensional periodically driven systems (in the absence of any additional symmetry besides particle number conservation) is the winding number W_{k_z} , which depends on the quasienergy k_z . For each quasienergy k_z , the value W_{k_z} is equal to the number of chiral edge states at that quasienergy^{32,33}. To compute the winding number for $k_z = 0$, we first compute the Bott index of the Floquet band²⁷, which lies in the quasienergy interval $0 \leq k_z \leq \Omega/2$. This Bott index essentially counts²⁷ the number of chiral edge states that traverse the gap at $k_z = \Omega/2$ less the number of chiral edge states that traverse the gap at $k_z = 0$. In addition, we verify that for the range of m_δ shown in Fig. 4 ($m_\delta > 1.4$ cm^{-1}), the gap at $k_z = \Omega/2$ hosts a single chiral edge state for the entire range of parameters with no disorder. Therefore, we conclude that, throughout the range of parameters shown in Fig. 4g, a Bott index of 0 corresponds to a topological gap at $k_z = 0$ and a Bott index of 1 corresponds to a trivial gap at $k_z = 0$.

Decay length of the edge state. We extract the decay length of the edge state from the experimental data. To achieve this, we analyse the intensity profile of the light propagating along the edge. To average over the disorder potential, we integrate the intensity per pixel along a direction parallel to the edge, and obtain the averaged intensity as a function of distance from the edge. The intensity profile (Extended Data Fig. 1a) decays with increasing distance from the edge, with peaks at the waveguide positions. We fit the envelope of the intensity profile to an exponential decay, which results in a decay length of the edge state of 47 μm (Extended Data Fig. 1b). This length scale is much smaller than the system size (158 μm). This result demonstrates that the system is sufficiently large for us to have observed the edge state. We do not observe any light at the far edge of the sample (the edge opposite the point at which the straw meets the sample), which indicates that the system size is sufficiently large that there is no considerable coupling between edge states on opposite sides.

We compare the experimentally obtained value of the decay length of the edge states with theoretical values obtained from a numerical simulation of a tight-binding model. The simulations are run for lattices with 60×30 unit cells with periodic

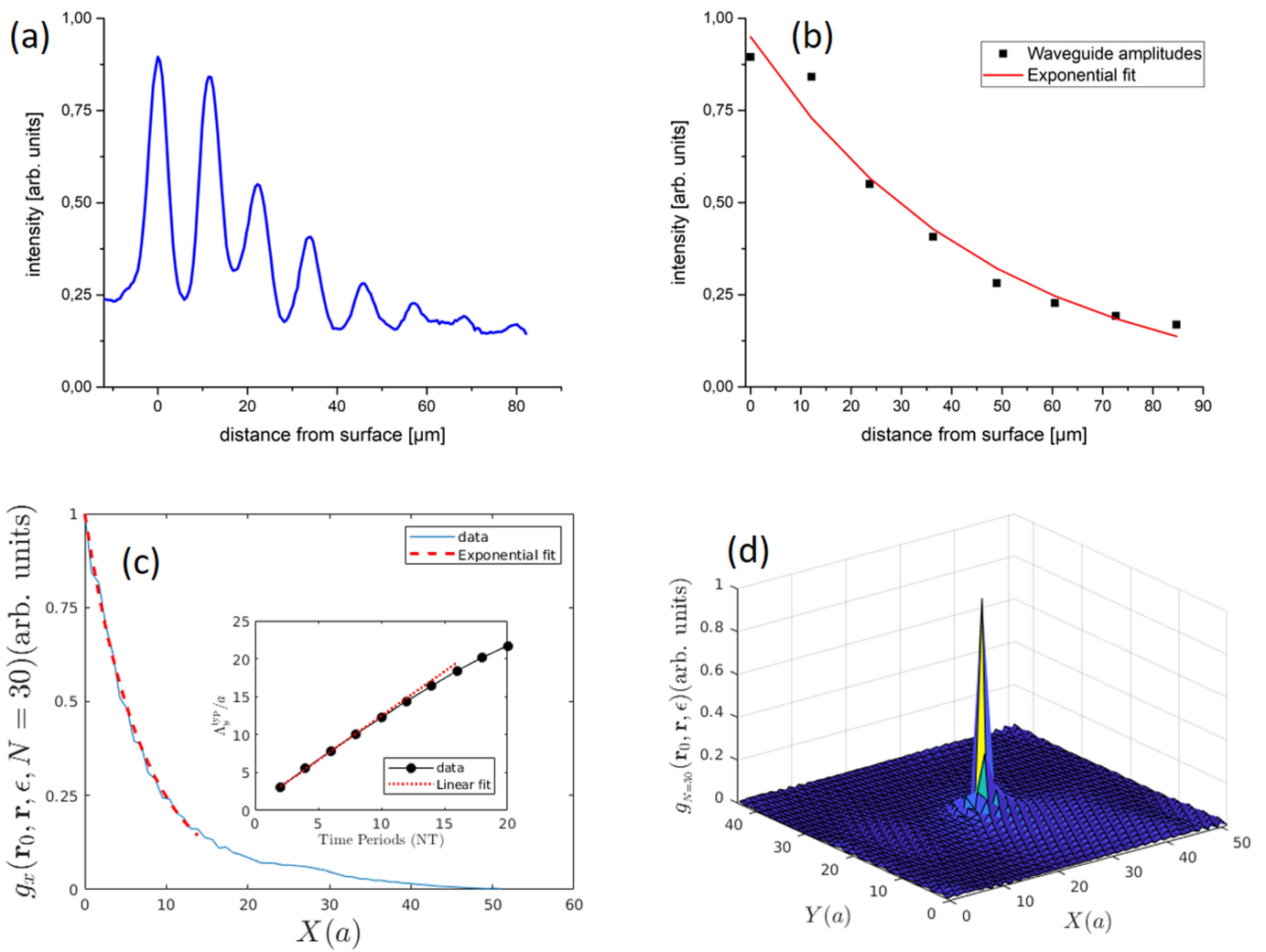
boundary conditions along y and open boundary conditions along x for a total time of $N = 30$ periods of rotation of the helices. The parameters for the tight-binding model are chosen as $c = 1.8$ cm^{-1} , $c_{\text{nnn}} = 0.234$ cm^{-1} , $m_\delta = 1.6$ cm^{-1} , $\Omega = 2\pi$ cm^{-1} , $kR\Omega a = 1.26$ and $w = 1.6$ cm^{-1} , where c_{nnn} is the next-nearest-neighbour hopping strength. To extract the decay length from the numerical simulation, we numerically compute the Green's function $G_N(\mathbf{r}_0, \mathbf{r}, NT) = \langle \mathbf{r} | U(t = NT, 0) | \mathbf{r}_0 \rangle$, where $U(t = NT, 0)$ is the evolution operator over N periods. From the Fourier transform of the Green's function in time, we compute $g_N(\mathbf{r}_0, \mathbf{r}, \varepsilon) = \langle |G_N(\mathbf{r}_0, \mathbf{r}, \varepsilon)|^2 \rangle$, where the angle brackets denote averaging over multiple realizations of the disorder. (For more details on the definition of these quantities, see ref. 27; in short, $U(t, t_0)$ is the time-dependent propagator from time t_0 to t , $|\mathbf{r}_0\rangle$ and $|\mathbf{r}\rangle$ are position eigenstates and ε is the quasienergy, equivalent to k_z in the experiment.) For initial positions \mathbf{r}_0 localized on the edge and ε in the mobility gap (near quasienergy $\varepsilon = 0$), the function $g_N(\mathbf{r}_0, \mathbf{r}, \varepsilon)$ shows propagation along the edge and an exponentially localized profile confined to the edge. We integrate $g_N(\mathbf{r}_0, \mathbf{r}, \varepsilon = 0)$, averaged over 100 realizations, along the direction parallel to the edge (that is, we integrate over the y component of \mathbf{r}). We extract the decay length from the decay profile of the result (which is a function of only the distance from the edge). The results (Extended Data Fig. 1c) give a decay length of $7a$.

From our numerical simulations, we can also extract the group velocity along the edge. This is achieved by examining the dependence of g_N , averaged along the x direction (perpendicular to the edge), as a function of time. The spread of this function along the y direction (parallel to the edge) can be quantified using a typical length scale³⁶ $\Lambda_y^{\text{DP}}(N)$, which is obtained by examining the inverse participation ratio of the disorder-averaged Green's function (integrated over the x direction)³. In the inset of Extended Data Fig. 1c, we show the dependence of $\Lambda_y^{\text{DP}}(N)$ on N , which clearly shows a linear growth indicating the ballistic nature of the edge state. The slope gives the velocity, which is $1.2a$ cm^{-1} .

From the numerically obtained disorder-averaged Green's function, we also extract the localization length of the bulk states. We take an initial position \mathbf{r}_0 in the bulk of the system and plot the corresponding function $g_N(\mathbf{r}_0, \mathbf{r}, \varepsilon) = \langle |G_N(\mathbf{r}_0, \mathbf{r}, \varepsilon)|^2 \rangle$ (Extended Data Fig. 1d). This yields a bulk localization length of $4a$. Our numerical analysis thus shows that quasienergies near $\varepsilon = 0$ are indeed in a mobility gap. Furthermore, the bulk localization length in the mobility gap near $\varepsilon = 0$ is indeed sufficiently smaller than the system size.

Data availability. All data generated or analysed during this study are available from the corresponding author upon reasonable request.

36. Titum, P., Lindner, N. H. & Refael, G. Disorder-induced transitions in resonantly driven Floquet topological insulators. *Phys. Rev. B* **96**, 054207 (2017).



Extended Data Fig. 1 | Experimental and numerical results for the disordered system. **a**, The averaged intensity profile of the edge state, which peaks at the waveguide positions. **b**, A fit through the waveguide peak intensities decays exponentially, with a decay length of $47\ \mu\text{m}$. **c**, The function $g_N(\mathbf{r}_0, \mathbf{r}, \epsilon)$, integrated along the edge, showing a decay length of

about $7a$. The inset shows the simulated displacement of the wavefunction along the edge for the parameters listed in Methods, from which the group velocity can be extracted. **d**, The function $g_N(\mathbf{r}_0, \mathbf{r}, \epsilon)$, for an initial position \mathbf{r}_0 deep in the bulk of the system, showing that the bulk localization length is approximately $4a$.